Article

Tetrahydroisoquinoline-Triazole Derivatives: Novel Nicotinamide *N*-Methyltransferase Inhibitors

Alison T. Ung * and **Matthew Payne**

School of Mathematical and Physical Sciences, Faculty of Science, University of Technology Sydney, Broadway, Sydney, NSW 2007, Australia; mwpn@novonordisk.com
* Correspondence: alison.ung@uts.edu.au

Abstract: Through the Lilly Open Innovation Drug Discovery program (OIDD), we discovered five cationic bis(aryltriazol-4-yl)methyl)-6,7-dimethoxytetrahydroisoquinolinium derivatives that effectively inhibit human nicotinamide N-methyltransferase. Compounds **4a**, **4c**, and **4f** demonstrated activity against hNNMT in enzymatic-based testing, with IC_{50} values of 3.177 μM, 7.9 μM, and 4.477 μM, respectively. In cell-based testing, **4c** and **4f** inhibited the enzyme in HEK293 cells with an IC_{50} value of 2.81 μM and 1.97 μM. Compound **4m** inhibited hNNMT in the enzymatic-based assay by 98% at a concentration of 10 μM, with IC_{50} of 1.011 μM in the cell-based assay. Through structure-activity relationship analysis, we found that the active compounds had electron-withdrawing substituents at the 4-position of the phenyl-triazole, while compounds containing bulky and electron-donating groups at the same position did not display any activity. The results of docking studies using AutoDock 4.2 showed that all active compounds had similar binding patterns at the NNMT active site. They occupied the nicotinamide binding site and about two-thirds of the *S*-adenosyl-L-methionine site. However, the SAR and docking results of **4g** contradicted the compound's inactivity. Nevertheless, the molecular docking studies provided insight into how the ligands interact with the protein and explained the activity of our compounds.

Keywords: bis(phenyl-triazolyl)-dimethoxytetrahydroisoquinolinium; hNNMT inhibitors; *S*-adenosyl-L-methionine (SAM); nicotinamide (NA); SAR; resistant cancers; metabolic disorders

1. Introduction

Nicotinamide *N*-methyltransferase (NNMT) enzyme is crucial in detoxification and energy metabolic pathways [1]. It is primarily expressed in the liver and, to a lesser extent, in other organs and adipose tissue [2,3]. NNMT facilitates the transfer of a methyl group from *S*-adenosyl-L-methionine (SAM), a methyl donor, to nicotinamide (NA), a recipient, resulting in the production of *S*-adenosyl-L-homocysteine (SAH) and *N*-methyl-nicotinamide (MNA), as illustrated in Scheme 1.

Additional roles of NNMT involve a range of disease status and physiological processes, including Parkinson's disease [4,5], numerous cancers [6–9] and metabolic disorders (e.g., Type 2 diabetes) [10–12]. Studies in animals and humans have linked the increased NNMT expression and activity in cancer cells with chemotherapy and radiation resistance and increased tumour aggressiveness [13].

Growing evidence suggests that NNMT may serve as a potential biomarker for tumour diagnosis and a new therapeutic target [13–15]. Downregulating or silencing NNMT has been shown to increase the sensitivity of cancer cells to radiation therapy, decrease tumorigenicity and induce apoptosis in cancer cells [16]. These findings provide critical support for the role of NNMT in treatment resistance in cancer cells. Therefore, compounds that can inhibit the activity of NNMT may have therapeutic value in cancer treatment. Only a few known NNMT inhibitors have been reported in the literature [17–24].
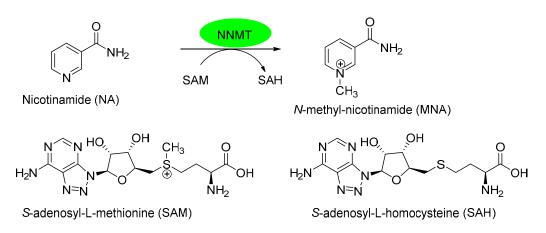
Scheme 1. Methylation of NA by NNMT using SAM as the methyl donor to form MNA and SAH.

There is an opportunity to develop novel NNMT inhibitors into molecular probes for mechanistic investigations and for developing therapeutic drugs for treating aggressive cancers in combination or monotherapy. Interestingly, NNMT is also overexpressed in the adipocyte cells of obese and diabetic mice, and overexpression of NNMT mRNA has been found in humans living with insulin-resistant type-2 diabetes (T2D). Therefore, compounds that can inhibit the activity of NNMT in the setting of metabolic pathways may have therapeutic utility in treating obesity and related chronic metabolic diseases [10,11,21]. Gao et al. emphasised the significance of developing cell-active inhibitors for NNMT, highlighting the need for research in this field [23]. In this publication, we report the inhibitory activity of our synthesised cationic bis(aryltriazol-4-yl)methyl)-6,7-dimethoxytetrahydroisoquinolinium compounds [25] against the human NNMT (hNNMT) enzyme as well as a molecular docking study to help explain the structure-activity relationship (SAR) requirements.

2. Materials and Methods

2.1. Biological Assay

Compounds listed in Table 1 (in Section 3.1) underwent screening through the Lilly OIDD program [26] to target hNNMT. The screening process involved primary and secondary assays using a workflow, as shown in Figure S1 of the Supplementary Information.

2.1.1. Primary Assays

hNNMT enzymatic modulation LC/MS assay single point (SP) (% Inhibition) concentration and hNNMT enzymatic modulation LC/MS assay curve respond concentration-response curve (CRC) (IC_{50}) were carried out by OIDD (Lilly Research Laboratories, Eli Lilly and Company, Indianapolis, IN, USA) [26] using a known method developed by van Haren et al. [27]. During the primary assays, the compounds were tested at a concentration of 10 μM using the hNNMT enzymatic modulation assay [27]. Ultra-High Performance (UHP) Hydrophilic Liquid Interaction Chromatography (HILIC) with Quadrupole Time-Of-Flight Mass Spectrometry (QTOF-MS) system was utilised to measure NNMT activity. A mass spectrometric-based detection system was effectively utilised to identify and measure MNA and SAH by-products. An internal standard d3-MNA and a positive control Sinefungin were used. The accuracy and precision of the MNA analysis were established within a range of 0.31–100 μM for both within and between run measurements. The calibration curve's linearity, sample recovery and detection limit were also confirmed.

2.1.2. Secondary Assays

Compounds **4a**, **4c**, **4f** and **4m** underwent hNNMT inhibitor cell-based assay in HEK293 (ATCC-CRL-1573) human hepatoma cell line. The assay was carried out by OIDD (Lilly Research Laboratories, Eli Lilly and Company, Indianapolis, IN, USA) using the method described in the paper by Roberti et al. [28] or Yoshida et al. [24] SAM (Sigma

#A7007, St. Louis, MO, USA) and 5 mM NAM (Fluka #72340, Charlotte, North Carolina, NC, USA) or NA-d4 (CDN Isotopes #D-3457) were used as substrates. LC-MS was used to monitor the concentrations of SAM, NA, SAH, and MNA or MNA-d4. Compounds **4a**, **4c**, and **4f** underwent a cell viability assay conducted by OIDD. The data were determined via the percentage cell growth inhibition of basal-HEK293 cells (hNNMT-overexpressing HEK293 cells).

2.1.3. Biological Data

With their permission, the biological data used here were generated and made available through Lilly's Open Innovation Drug Discovery (OIDD) Program. The OIDD team performed the Analytical Method Validation and Data Analysis, and the provided data are considered statistically valid.

2.2. Molecular Docking Study

2.2.1. Ligands Preparation

To prepare for docking studies, the compounds **4a–n**, **MvH45**, and **MS2734** were constructed and optimised using Semi-Empirical (AM1) calculations from the setup menu in Spartan 10 (Wavefunction, Inc., Irvine, CA, USA). Once completed, all files were saved in mol2 format. These compounds were then further prepared using the "Preparing a Ligand for AutoDock" steps found in the "Using AutoDock 4 and Vina with AutoDockTools: A tutorial"—in AutoDock 4.2 with AutoDockTools (ADT, The Scripps Research Institute, San Diego, CA, USA) Version 1.5.7 interface [29]. Finally, each compound was saved in PDBQT format for AutoDock study.

2.2.2. Protein Structure Preparation

The hNNMT crystal structure was obtained in a complex with MS2734 (PDB ID: 6CHH) [19] from the RCSB Protein Data Bank. Before the docking studies, the original inhibitor **MS2734** was removed, along with water molecules. Any missing hydrogen atoms were added, and the protein was saved in the pdb file format using Discovery Studio (DS) Visualizer v21.1.0.20298 software (Dassault Systèmes BIOVIA: San Diego, CA, USA, 2020). The protein was further prepared in AutoDock 4.2 using the suggested steps for "Preparing the Macromolecule" [29–31]. First, polar-H atoms were added, followed by the addition of Kollman charges. Then, all non-polar hydrogen atoms were merged, and the "AD4 type" forcefield was assigned to atoms in the protein using the ADT "Edit" tool. This optimisation process corrected structural, atomic, and bond length anomalies and charge irregularities. The optimisation step was crucial in ensuring a stable conformation before saving the structure in PDBQT format for docking study.

2.2.3. Preparing Grid Parameters

The grid parameter file was set up for hNNMT (6CHH) and ligand using the recommended steps [29–31] in AutoDock 4.2. The active site was chosen as the grid box with $50 \times 50 \times 50$ points in x, y, and z dimensions and a grid box spacing of 0.375 Å. The grid box was centred at the binding coordinate of **MS2734**, where the x, y, and z centres were set at -8.417, -29.18, and 22.908, respectively. The grid output parameters were saved in a gpf file, which was utilised to run AutoGrid and generate grid glg and map files.

2.2.4. Preparing Docking Parameters

The docking studies were set up following the recommended steps in AutoDock 4.2 [29–31]. The macromolecule for docking was selected as "Set Rigid Filename". The search parameters for docking were set as Genetic Algorithm (GA) with the maximum number of evaluations set to "long" (25,000,000), 10 GA runs, and the remaining parameters were used as defaults. The docking output was saved as a dpf file and then used to run AutoDock. Upon successful completion of the AutoDock run, a results log (dlg file) was generated.
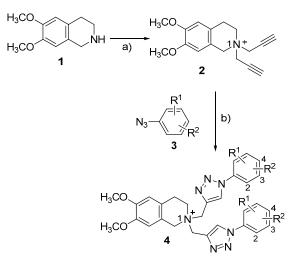
2.2.5. AutoDock Results Analysis

The results of ten genetic algorithm runs (in a dgl file) were analysed and ranked using the Analyze tool in ADT based on binding energy, clustering, and root-mean-square-deviation (rmsd) [29–31]. The conformation with the best energy ranking was chosen for further analysis of its protein-ligand interactions and other docking scores. In addition, DS Visualizer software was used to closely analyse the interactions between the inhibitors and the hNNMT binding site.

3. Results and Discussion

3.1. Synthesis of Inhibitors

We previously reported the synthesis of cationic bis(aryltriazol-4-yl)methyl)-6,7-dimethoxytetrahydroisoquinolinium derivatives **4** (Scheme 1) as antibacterial agents [25] using the nitrogen atom of dimethoxytetrahydroisoquinoline **1** to attach the terminal alkyne to produce compound **2**. We focused on changing R^2 structurally, with the introduction of R^2 achieved through the triazole ring formation in the final reaction step between the aromatic azide **3** and alkyne **2**. Using Cu-catalyzed azide-alkyne cycloaddition [32,33], we could incorporate various substituted aromatic rings by forming the triazole ring to obtain compounds, as illustrated in Scheme 2 and Table 1.

Scheme 2. Synthesis of cationic bis(aryltriazol-4-yl)methyl)-6,7-dimethoxytetrahydroisoquinolinium **4** [a] [25]. [a] Reagents and conditions: (a) Propargyl bromide (3 eq.), K_2CO_3 (4 eq.), CH_3CN, rt, 3 h; (b) aromatic azide **3** (2 eq.), sodium ascorbate (1 eq.), $CuSO_4.5H_2O$ (0.2 eq.), H_2O: *i*-PrOH (1:1), rt, 24 h.

Table 1. Compounds **4a–n**.

Compound	R^1	R^2
4a	H	H
4b	H	4-*tert*-butyl
4c	H	4-CF_3
4d	H	4-Ph
4e	H	4-Cl
4f	H	4-CN
4g	H	4-NO_2
4h	H	4-$CON(CH_3)_2$
4i	H	4-CH=CH-Ph
4j	3-F	4-OCH_2Ph
4k	2-F	4-OCH_2Ph
4l	H	4-CH_2OPh
4m	H	3-CH_2OPh
4n	H	4-CH_2SPh

3.2. Compounds Cheminformatic Evaluation Using OIDD in Silico Screening

The Lilly Open Innovation Drug Discovery (OIDD, Lilly Research Laboratories, Eli Lilly and Company, Indianapolis, USA) [26] program was an initiative by Lilly that encouraged collaboration with researchers globally. This program enabled scientists to use Eli Lilly's resources to screen new molecules while retaining intellectual property control. Compounds **4a–n** in Table 1 were first submitted for a cheminformatic evaluation using the OIDD platform [26]. They were selected for their novelty and drug-like properties based on cheminformatic evaluation. The submitted molecular structures were analysed using filters to select compounds with strong druggable features and eliminate any that may interfere with biological assays during screening. These filters included MW, cLogP, solubility, toxicity, and other physicochemical properties. After undergoing cheminformatic evaluation, the molecules were subject to a substance check and compared with known drugs from both Lilly and PubChem collections. This was done to ensure that only novel compounds were selected. Once the selection was made, the molecules listed in Table 1 were sent to Lilly for a high throughput screening study against key therapeutic targets in the OIDD program. Among the tested targets, our compounds showed inhibitory activity against hNNMT.

3.3. Biological Activities Novel NNMT Inhibitors

Compounds listed in Table 1 underwent screening through the Lilly OIDD program [26] to target hNNMT. The screening process involved primary and secondary assays using a workflow, as shown in Figure S1 of the Supplementary information. The primary assays screened the compounds at a single point (SP) concentration to determine their percentage inhibition (%). Compounds with greater than 50% inhibition were selected for hNNMT enzymatic modulation assay concentration-response curve (CRC, IC_{50}) assay. Compounds with good IC_{50} values were then tested in secondary assays, which involved determining their inhibitory activity against hNNMT in a cell-based assay and their toxicity in a cell viability assay.

During the primary assays, compounds were tested at a concentration of 10 μM using an hNNMT enzymatic modulation UHP-HILIC-MS assay created by van Hare et al. [27]. The system used a mass spectrometric-based detection system to identify and measure MNAand SAH by-products. An internal standard of d3-MNA and positive control Sinefungin were utilised. The linearity of the calibration curve, sample recovery and detection limit were also verified.

The inhibitory activity of all compounds listed in Table 1 at a concentration of 10 μM is provided in the Supplementary Information Table S1. In the primary assays, **4a, 4c, 4f, 4h**, and **4m** were found to have inhibition greater than 50% against hNNMT, as noted in Table 2. **4b** was able to inhibit the enzyme at a lower percentage of 40%. Following this, **4a, 4c, 4f**, and **4h** were further tested for their IC_{50} values in the MNA and SAH concentration-response curves (Table 2). The results obtained from detecting MNA and SAH showed comparable percentages of inhibition and IC_{50} values. MNA concentration-response curves of tested compounds are shown in Figure 1, and their SAH concentration-response curves are provided in Supplementary information in Figure S2.

To assess their effectiveness, compounds **4a, 4c, 4f**, and **4m** underwent the secondary assay in which they were tested for their ability to inhibit hNNMT overexpression in HEK293 cells. The results showed that **4a** inhibited the enzyme in HEK293 cells with an IC_{50} value of 21.75 μM (Figure 2A), indicating that its activity against hNNMT in HEK293 cells was less effective than in the enzymatic-based assay. However, **4c** and **4f** performed slightly better in the cell-based assay than in the enzymatic-based assay, with IC_{50} values of 2.81 μM and 1.97 μM, respectively (Figure 2B,C). At a concentration of 10 μM, **4m** inhibited hNNMT in the enzymatic-based assay by 98%. Although its IC_{50} was not determined in the enzymatic-base assay by the OIDD team, a subsequent investigation in the cell-based assay indicated an IC_{50} of 1.011 μM (Figure 2D).

Table 2. Inhibitory activity of compounds **4a**, **4b**, **4c**, **4f**, **4h** and **4m** against hNNMT.
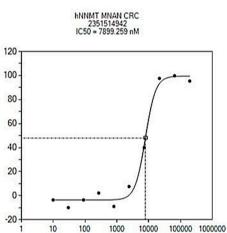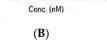
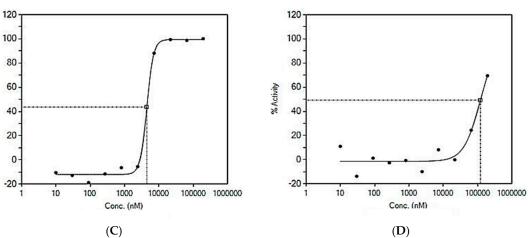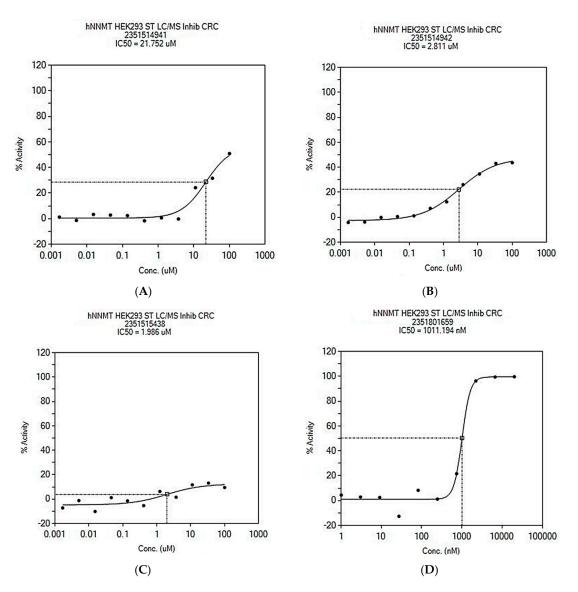| Compound	hNNMT MNA, % Inhibition (%) at 10 μM	hNNMT SAH, Inhibition (%) at 10 μM	hNNMT MNA, IC_{50} (μM)	hNNMT SAH, IC_{50} (μM)	hNNMT in HEK293, IC_{50} (μM)
4a	91.29	89.73	3.177	3.207	21.75
4b	40.09	40.16	ND	ND	ND
4c	58.68	56.76	7.9	8.035	2.81
4f	86.74	87.21	4.477	4.389	1.97
4h	99.34	99.13	121.6	134.5	ND
4m	97.99	97.99	ND	ND	1.011

ND: Not determined.

Figure 1. Concentration-response curve (CRC, IC_{50}) of hNNMT enzymatic modulation using LC/MS assay via monitoring MNA (MNAN) production for (**A**) **4a**, (**B**) **4c**, (**C**) **4f** and (**D**) **4h**. Please note that the OIDD team used the term "MNAN" to refer to "MNA".

Figure 2. Inhibitory of hNNMT overexpressed in HEK293 cells, Concentration-response curves (CRC, IC_{50}) of hNNMT enzymatic modulation using LC/MS for (**A**) **4a**, (**B**) **4c**, (**C**) **4f** and (**D**) **4m**.

According to the cell viability assay, compounds **4a**, **4c** and **4f** showed no toxicity towards basal-HEK293 cells, even at the highest test concentration of 100 μM. The percentage growth inhibition observed in basal-HEK293 cells indicated cell viability of approximately 100%, as depicted in Supplementary Figure S3. Based on these results, our lead compounds have the potential for the development of potent and selective hNNMT inhibitors.
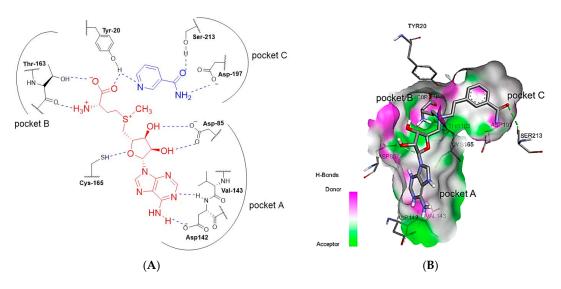
3.4. SAR Analysis

Out of the 14 compounds that were tested, five (Table 2) of them showed effectiveness against hNNMT. Among these, **4a**, **4c**, **4f** and **4h** have small R^2 substituents such as H, CF_3, CN, and $CON(CH_3)_2$ at the 4-position of the aromatic ring. CF_3, CN, and $CON(CH_3)_2$ are electron-withdrawing groups. On the other hand, the molecules **4e** and **4g**, which also contain the electron-withdrawing groups (Cl and NO_2), did not show any inhibition of hNNMT. In contrast, compounds **4d**, **4i**, **4j**, **4k**, **4l,** and **4n** have large electron-donating R^2 at the 4-position of the aromatic ring and were found to be inactive. It is essential to emphasise that compound **4m** is one of the five active compounds. **4m** distinguishes itself from the other four active compounds by having R^2 as a large electron-donating group (-CH_2OPh) in the 3-position of the aromatic ring rather than a small electron-withdrawing group at the 4-th position. Neelakantan et al. [17] conducted a structural activity relationship (SAR)

study of nicotinamide-competitive inhibitors and found that the cationic nitrogen group is a crucial pharmacophoric feature. The cationic nitrogen feature perhaps contributes to the activity observed in our compounds. While these results are not comprehensive, they provide some insight into the structural activity relationship (SAR) needed for activity against hNNMT. In order to better understand how our inhibitors interacted with hNNMT and achieved inhibitory activity, we conducted a molecular docking study of our compounds using the published crystal structure of hNNMT (PDB ID: 6CHH) [20] and AutoDock 4.2 software (version 4.2.6) [34].
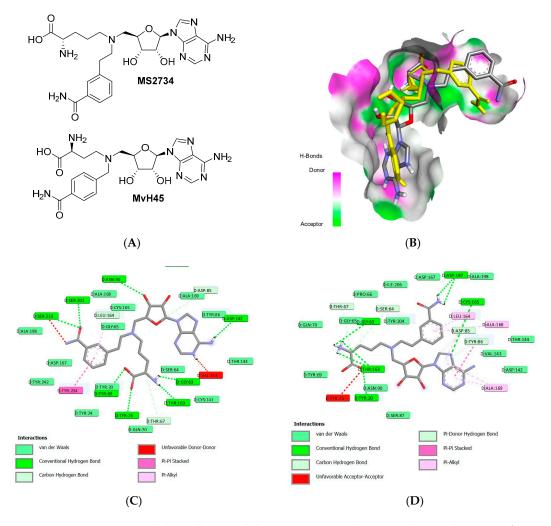
3.5. Molecular Docking

The published crystal structures of hNNMT can facilitate the rational design of new NNMT inhibitors [19–21]. The crystal structures reveal the interactions of the substrates with the active site residues [18]. There are three defined sub-pockets in the NNMT active site: the adenine and sugar unit (pocket A), the homocysteine moiety (pocket B), and the nicotinamide unit (pocket C), as shown in Figure 3. The 2D diagram in Figure 3A illustrates the interactions of NAM and SAM with the protein receptor. The NAM structure binds to pocket C and interacts with ASP197 and SER213, while SAM occupies adjacent pockets B (TYR20 and THR163) and pocket A (Val143 and Asp142).

(**A**) (**B**)

Figure 3. (**A**) The active site adapted from the crystal structure of human NNMT [18], (**B**) showing the bindings of a bisubstrate NNMT inhibitor **MS2734** (PDB 6CHH—generated in DSVisualizer), detailed interactions between the inhibitor and the binding pockets' amino acid residues [20].

The hNNMT crystal structure in complex with the bisubstrate inhibitor **MS2734** (PDB ID: 6CHH) [20] offers detailed interactions necessary for inhibition. **MS2734** (Figure 4A) is a competitive inhibitor of SAM and a non-competitive inhibitor of NAM, with an IC_{50} value of 14 μM in enzymatic assay. It binds to both SAM and NAM binding sites. As shown in Figures 3B and 4C, the amino acid side chain binds deeply into pocket B and forms H-bonds with TYR25, TYR69, GLY63, THR163 and THR67 with close contact with SER64 and TYR20. The ribose hydroxyl groups also form hydrogen bonds (H-bonds) with ASP85, ASN90 and CYS165 in the space between pockets B and A. The adenine component of **MS2734** sits in pocket A, forms H-bonds with VAL143 and ASP142 and is in close contact with TYR86 and ALA169. The 3-aminophenyl group occupies pocket C and forms H-bonds with SER201 and SER213. It also forms π-π stacking and pi-interactions with LEU164 and TYR204, respectively, and is in close contact with ALA168 and ASP197.

Figure 4. (**A**) Bisubstate inhibitors **MS2734** and **MvH45**, (**B**) 3D diagrams of interaction between best re-docked conf-6 (yellow) and the active site demonstrated by overlapping with **MS2734** in the crystal structure (6CHH), (**C**) 2D ligands-receptor interactions of **MS2734** in X-ray structure (6CHH) and (**D**) 2D ligands-receptor interactions of best re-docked conf-6 at the active site (6CHH).

3.5.1. Docking Method Validation

The crystal structure of hNNMT in complex with the inhibitor **MS2734** (PDB ID: 6CHH) [20] was obtained from the RCSB Protein Data Bank. To prepare the protein structure for docking studies, AutoDockTools (Version 1.5.7) [31] and AutoDock 4.2 [34] used the protocol as detailed in the experimental method. To validate the docking protocol, the minimised structure of **MS2734** was redocked into its original binding site in the X-ray structure. The results of 10 Genetic Algorithm runs of the redocking were analysed, ranked, and presented in Table 3. The best docking score of **MS2734** was achieved by redocked conformation 6 (redocked-conf-6), with a binding energy of -11.29 kcal/mol.

The position, orientation, conformation, and interactions of the redocked **MS2734** were compared to those of the original X-ray structure (PDB ID: 6CHH) at the binding site. It is worth noting that the redocked-conf-6 assumed a slightly different shape in specific parts of the molecule, namely the adenine and sugar unit (pocket A) and nicotinamide unit (pocket C), as depicted in Figure 4B, compared to its structure in the X-ray structure (6CHH). The variation in conformation is perhaps due to the stable conformation of the redocked-conf-6 adopted in silico.

Table 3. Hydrogen bond interactions between **MS2734** and redocked-**MS2736** in hNNMT (6CHH).

MS2734	Binding Energy (kcal/mol)	H-Bonds	Amino Acids Involved in Hydrogen Bonding		
			Pocket A	Pocket B	Pocket C
In X-ray structure (6CHH)	NA	11	ASP42, VAL143, ASN90, CYS165, ASP85	TYR25, TYR69, GLY63, THR163, THR67,	SER213, SER201, LEU164
redocked-conf-6	−11.29	11	CYS165, ASN90, TYR86	TYR20, THR163, GLY63, THR67, SER64	ASP197
redocked-conf-2	−8.52	3	ASN90	GLY63, THR163,	
redocked-conf-7	−7.91	3	ASN90	THR163, GLY63,	
redocked-conf-8	−7.7	4	VAL143, ASN90	THR163, GLY63,	
redocked-conf-3	−6.76	3	VAL143	TYR69, TYR204	
redocked-conf-10	−6.5	3	VAL143, ASN90	ANS16	
redocked-conf-9	−6.26	0	-	-	
redocked-conf-1	−5.52	1	ASP85		
redocked conf-4	−4.95	3	ASN90, ASP85	-	SER201
redocked-conf-5	−4.71	1	-	ASN16	-

In comparison to **MS2734** found in the crystal structure, the redocked-conf-6 established 11 H-bonds with two out of five shared residues in pocket A (CYS165, ASN90), four out of six shared residues in pocket B, and one out of two shared residues in pocket C. The amino acid side chain of the redocked-conf-6 formed H-bonds with TYR20, THR163, GLY63, SER64 and THR67 in pocket B. Within pocket A, the adenine and sugar unit formed H-bonds with CYS165, TYR86 and ASP85 and formed van der Waals interactions with the key residues ASP142 and VAL143. Additionally, the 3-aminophenyl group formed a H-bond with ASP197, pi-interactions with LEU164 and ALA168, and closed interactions with TYR204 in pocket C, as shown in Figure 4D. The shared vital interactions are shown in Table 3. This indicates that the redocked-conf-6 could recognise its original receptor site in the X-ray structure of 6CHH using this docking protocol. The results above validated the docking protocol as a suitable method for this study [35].

MvH45 (Figure 4A) is another bisubstrate hNNMT inhibitor with an IC_{50} of 29.2 μM [18]. It was used in the docking study as a standard compound, along with **MS2734**, for comparative study and to confirm our validated method. The docking results reveal that the amino acid side chain of **MvH45** bound deeply into pocket B and interacted with critical amino acid residues such as TYR20, THR163 and GLY63. The ribose hydroxyl group formed an H-bond with ASN90, while the adenine nitrogen formed an H-bond with ASP95. It can be inferred from the interactions observed that the adenine unit was bound to the upper region of pocket A (as indicated in Supplementary Table S2). On the other hand, the 3-amidophenyl unit was well-bound in pocket C, which is characterised by its interactions with ASP197, SER213, and TYR204). The docking results of **MvH45** further validate the suitability of our docking method (Table 4).

3.5.2. Docking Scores of 4a–n

The validated docking protocol was used to determine compounds **4a–n** in silico for their ability to dock into the active site of the hNNMT. The efficacy of inhibition was determined based on the binding energy (kcal/mol) of the compounds, which was expressed as Gibbs-free energy. Compounds with higher negative binding energy were considered better inhibitors [36]. Estimate ligand efficiency and inhibitory constants are also part of the docking score, as shown in Table 4.

Table 4. Docking results of compounds **4a–n**, **MS2734** and **MvH45** with the hNNMT (6CHH).

Compound	Binding Energy (kcal/mol)	Predicted Ligand Efficiency	Predicted Inhibition Constant	Exp IC$_{50}$ (µM) [a]
MS2734	−11.29	−0.3	5.32 nM	14.4
MvH45	−11.32	0.31	5.05 nM	29.2
4a	−12.9	−0.34	350.2 pM	3.2
4b	−11.73	−0.26	2.52 nM	NA
4c	−11.62	−0.25	3.03 nM	7.9
4d	−9.97	−0.2	49.45 nM	NA
4e	−13.16	−0.33	227.46 pM	NA
4f	−12.42	−0.3	793.31 pM	4.477
4g	−11.91	−0.27	1.87 nM	NA
4h	−11.95	−0.25	1.75 nM	121.6
4i	−11.73	−0.22	2.51 nM	NA
4j	−9.94	−0.18	51.79 nM	NA
4k	−9.86	−0.18	59 nM	NA
4l	−6.96	−0.13	7.9 µM	NA
4m	−11.45	−0.21	4.07 nM	1.1 [b]
4n	−8.61	−0.61	487.35 nM	NA

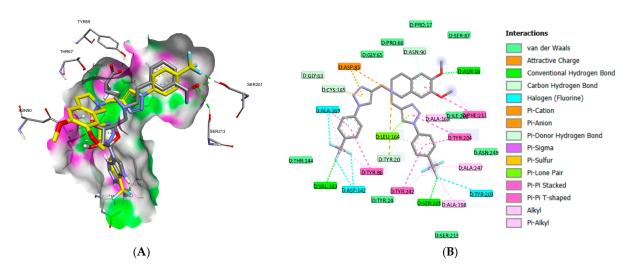NA: non-active; [a]: from enzyme-based assay; [b]: from cell-based assay.

The docking scores presented in Table 4 indicate that the active compounds listed in Table 2, including **MvH25**, have binding energies lower than −11 kcal/mol. However, inactive **4e**, **4g**, and **4i** have binding energies of −13.16, −11.91, and −11.73 kcal/mol, respectively. **4e** and **4g** have small electron-withdrawing substituents (Cl and NO_2) at the 4-position of the aromatic ring. The electron density of these aromatic rings is comparable to that of **4c**, **4f**, and **4h**. Therefore, the effect of pi-interactions, especially with tyrosine residues, would be expected to be similar. The electronic effect of these electron-poor aromatic rings may be the reason behind the low binding energies of **4e** and **4g**. However, no correlation was found between structure and the low binding energy of the inactive **4i**. Analysis of interactions between the compounds at the hNNMT active site can help to explain these anomalies.

3.5.3. Ligand Interactions Analysis

DS Visualizer was used to analyse H-bonds and visualise the binding interactions between hNNMT and compounds **4a–n**. The results, including the number of H-bonds, the residues involved in these interactions, and other favourable interactions, are summarised in Table 5 and Supplementary Table S2. The 4-CF$_3$-phenyl-triazolyl part of **4c** completely occupied pocket A. The CF$_3$ group formed H-bonds with key amino acid residues VAL143 and ASP142, and the aromatic ring formed H-bond and pi-pi stacking with CYS165 and ASP85, respectively. The triazole ring occupied the sugar-binding pocket and formed H-bonds with ASP85 and GLY63. The dimethoxytetrahydroisoquinolinium (DMTHIQ) core occupied the front part of pocket B. This moiety formed attractive charge interactions with ASP85 and TYR20, with the aromatic ring forming a hydrogen bond with ASN90 and the OCH$_3$ group forming a hydrogen bond with ASN16. However, no hydrogen bonds were observed with the key residues TYR25, TYR69, THR163, and THR67 at the back of pocket B. To illustrate that the DMTHIQ core and a 4-CF$_3$-phenyl-triazolyl component of compound **4c** could occupy approximately two-thirds of the SAM binding site, the docking structure of **4c** was superimposed over the **MS2734** in the crystal structure (6CHH), as shown in Figure 5A. The second 4-CF$_3$-phenyl-triazolyl component of **4c** fitted well into pocket C (nicotinamide pocket). The CF$_3$ group formed hydrogen bonds with SER201, while the aromatic and triazole rings formed important pi-pi stacking interactions with TYR204 and TYR242. The triazole ring was also involved in pi-interaction with LEU164, as shown in Figure 5B.

Table 5. Amino acids involved in the interactions between hNNMT (6CHH) and **MS2734**, **MvH45** and **4a–n,** respectively.

Compound	Hydrogen Bonding				Attractive Charge and pi-Interactions
	Number	Pocket A	Pocket B	Pocket C	
MS2734 X-ray structure (6CHH)	11	ASP142, VAL143, ASN90, CYS165, ASP85	TYR25, TYR69, GLY63, THR163, THR67	SER213, SER201, LEU164, TYR204	TYR204
MS2734 redocked	11	CYS165, ASN90, TYR86	TYR20, THR163, GLY63, THR67, SER64	ASP197	LEU164, ALA169, ALA168
MvH45	10	ASP85, ASN90	TYR20, GLY63, THR163	ASP197, SER213	TYR204, ALA168, ALA169, LEU164
4a	5	CYS165, ASN90, ASP85		SER201, LEU164	VAL143, ALA169, ALA168, ASP85, PRO17, PHE211,TYR204, ALA198, TYR242
4b	2			TYR204, LEU164	CYS165, TYR68, ALA169, ALA168, ILE206, ALA198, TYR242
4c	13	VAL143, ASP142, ALA169, CYS165, ASP85, ASN90	TYR20, ASN16, GLY63, SER87, ASN16	SER201, TYR203, TYR204, LEU164, ALA198	ASN85, TYR86, PHE211, AL168, TYR204, TYR242, ALA198, ALA247
4d	3	CYS165	TYR20	TYR204	VAL143, LEU164, TYR204, ALA198, CYS141
4e	4	ASN90, ASP85		LEU164	VAL143, ALA169, CYS165, TYR20, PRO17, ALA168, TYR204, ALA198, TYR242
4f	9	VAL143, CYS165, ASN90, ASP85, TRY86	ASN16, TYR20,	SER201, SER213, ASP197, LEU164 TYR204	ALA169, PRO17, ALA168,
4g	7	VAL143, CYS165, ASA90, ASP85	ASN16, TYR20,	SER213, LEU164	TYR86, ALA169, ALA168, ALA198
4h	8	ASP142, ASN90, ASP85, THR144	ASN16, GLY63, TYR20	TYR204, TYR24, LUE164	PHE211, ALA169
4i	1	CYS165			ASP85, ALA169, TYR20, ASN16, LEU164, ALA168, TYR204
4j	6	CYS165, ASN90	ASP16, TYR20,	LEU164	ASP85, VAL143, ALA169, PRO17, PHE211, ALA198
4k	5	ASP142, ASP85	TYR24, PRO17		LEU164, TYR204, CY165, ASP90
4l	2	VAL143, SER87			ASP142, ALA169, CYS165, TRY204, LEU164, ALA198
4m	8	ASP85, ASN90, CYS165, TYR86, ASP142	ASN16, TYR20	LEU164, TYR204	ALA198, TYR247, ALA168, TYR20, PHE211, ILE206, ALA169
4n	5	ASN90, CYS165	THR163	LUE164	TYR204, ALA198, ALA168, ALA169

(A) **(B)**

Figure 5. (**A**) Structural alignment of **4c** (yellow stick) and **MS2734** (grey stick) within the active site of NNMT (6CHH), (**B**) 2D ligands-receptor interactions of **4c** at the active site (6CHH).

In their 2021 study, Gao et al. [22] emphasised the effectiveness of electron-deficient aromatic groups in forming pi-pi stacking between hNNMT's tyrosine residue TYR204 in pocket C. This interaction is required for the potency increase of bisubstate inhibitors. It is worth mentioning that Roberti and colleagues [28] discovered a tetracyclic steroid called CC-410 that is effective against hNNMT, with an IC_{50} of 1.6 µM. The docking study of CC-410 revealed that it could act as a bisubstrate NNMT inhibitor by binding near the opening of the active site. Part of the molecule filled the NAM pocket, while the remaining part of the molecule partly occupied the SAM pocket.

The docking results revealed that compounds **4a**, **4e**, **4f**, **4g** and **4h** have similar binding conformation and orientation to that of **4c** (Table 5 and Supplementary Table S2). The active compounds **4a**, **4c**, **4f**, and **4h** showed hydrogen bonding with important amino acids at NNMT active sites. However, compound **4e** was mainly found to bind weakly into pockets A and C. In pocket A, the 4-Cl-phenyl-triazole component formed a H-bond with AS90 and pi-anion interaction with ASN85. Other weaker pi-interactions were also observed between the 4-Cl-phenyl-trizole and TYR86, VAL143, ALA169 and CYS165. The cationic nitrogen of DMTHIQ formed attractive charges with ASP85 and TYR20. The second 4-Cl-phenyl-triazole component formed a H-bond with LEU 167 and π-π stacking with TYR204 and other weak pi-interactions with ALA168, TYR242, ALA198 and TYR242. These weak interactions may explain its inactivity against hNNMT.
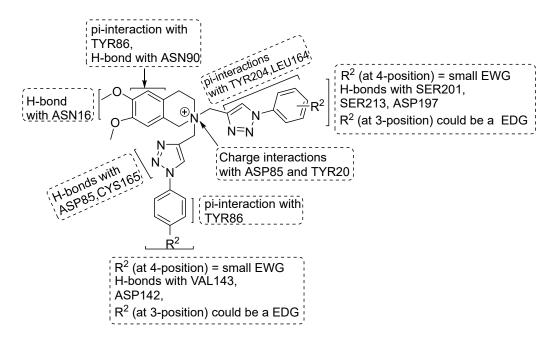
In contrast, the inactive compound **4g** displayed similar hydrogen bonding interactions and docking scores to those in the active compounds. Compound **4g**'s docking results suggest it is an active inhibitor. However, it failed to show inhibition against NNMT, possibly due to bioavailability issues in the primary assay conducted by OIDD. At a concentration of 10 uM, compound **4b** could only inhibit 40% of the enzyme activity (Table 5 and Table S2). The compound could partially bind to pockets A and C, leaving pocket B unoccupied. This was due to the sizeable electron-donating *tert*-butyl group, which created an electron-rich, bulky 4-substituted aromatic ring that could not fit into pocket C. As a result, pocket C was unfavourably occupied by the DMTHIQ core. One of the 4-*tert*-butyl-phenyl-triazole moieties occupied the top position of pocket A, while the other was bound unfavourably to an undefined pocket located at the front-right side of pocket A. These binding characteristics were also found in compounds **4d**, **4i**, **4j**, **4k**, **4l** and **4n**. These compounds have large electron-donating substituents at the 4-position of phenyl-triazole, making these components too bulky and electron-rich to dock and form favourable interactions with any of the pocket B, C or A. Compounds **4d**, **4l**, and **4i** were found to have intramolecular π-π stacking between their aromatic and triazole rings (Table S2). These interactions caused a decrease in the entropy of the ligand, which resulted

in the stabilisation of its binding and a lowering of binding energy. This led to the formation of a compact or folded conformation, which prevented the molecules from interacting with crucial amino acid residues required for NNMT inhibition. This intramolecular interaction and conformation can explain the lower binding energy and inactivity of compound **4i** [37]. Moreover, the inactivity of compounds **4d**, **4l**, and **4i** could be attributed to the absence of SAM and NA binding motifs.

Compound **4m** has a sizeable electron-donation group at the 3-position of the phenyl-triazole. Based on the docking results, **4m** has a binding energy comparable to other active compounds. It also formed intramolecular pi-pi stacking interaction between the two triazole rings and adopted compact conformation. Comparatively, the electron density in the phenyl-triazole group is lower than that of **4d**, **4i**, **4j**, **4k**, **4l**, and **4n**. Due to its bulky R^2, **4m** could only occupy pockets A and C and form necessary hydrogen bonding interactions with the key amino acid residues at the active site (Table 5 and Table S2).

3.6. Summary of SAR

Molecular docking results provide valuable insights into how our inhibitors interact with hNNMT, resulting in inhibitory activity. The SAR analysis of the active compounds has identified several key chemical features that are required for NNMT inhibition, as summarised in Figure 6. These include (i) the importance of the DMTHIQ core for interacting with ASP85 and AS90, (ii) the crucial role of the positive charge on the N atom of DMTHIQ for interacting with key residues ASP85 and TYR20, (iii) the requirement for R^2 (at the 4-position) to be polar, small, and EWG so that it can form H-bonds with crucial amino acids in the C (SER201, SER213, and ASP197) and A (VAL143 and ASP142) pockets, (iv) the need for the phenyl-triazole system to be electron-deficient to form pi-interactions with TYR204 and LEU164 in pocket C and TYR86 in pocket A, and (v) favourable electron-donating group (R^2) at the 3-position of the aromatic ring, such as the one observed in **4m**, could potentially be beneficial.

Figure 6. SAR summary for activecationic bis(aryltriazol-4-yl)methyl)-6,7-dimethoxytetra hydroisoquinoliniumderivatives.

4. Conclusions

The Lilly OIDD program has identified five compounds that effectively inhibit hNNMT. Compounds **4c**, **4f** and **4m** are effective against hNNMT. Compounds **4c**, **4f** and **4m** are effective against hNNMT in both enzyme- and cell-based assays at low micromolar

concentrations. Analysis of the SAR and docking study of this small set of molecules revealed that active compounds **4c**, **4f** and 4h have electron-withdrawing substituents at the 4-position of the aromatic ring. On the other hand, an electron-donating group (R^2) at the 3-position of the aromatic ring was found to be beneficial for the activity of compound **4m**. Conversely, molecules containing bulky and electron-donating groups at the 4-position of the aromatic ring did not show any activity. All active compounds have similar binding motifs at the NNMT active site. While compound **4g** did not show inhibition against NNMT in the primary assay conducted by OIDD, the SAR analysis and docking studies suggest that it should be active. Although the SAR of compound **4g** was not clear-cut, the molecular docking studies have provided some insight into the ligand-protein interactions and a plausible explanation for the activity of our compounds. It is crucial to highlight that our findings are preliminary and require further investigation. To achieve a comprehensive SAR, a diverse range of compounds around **4c** or **4m** needs to be synthesised. Obtaining more comprehensive biological data, including in-vitro pharmacokinetics data of the active compounds, would significantly enhance our understanding of the inhibitory activity of these compounds.

Supplementary Materials: The following supporting information can be downloaded at: https://www.mdpi.com/article/10.3390/appliedchem3040032/s1, Figure S1. Lilly OIDD hNNMT Flow Scheme and Assay Measures; Figure S2. Concentration-response curve (CRC, IC_{50}) of Nicotinamide *N*-methyltransferase (hNNMT) enzymatic modulation using LC/MS assay via monitoring *S*-adenosyl-L-homocysteine SAH production; for (A) **4a**; (B) **4c**; (C) **4f** and (D) **4h**; Figure S3. Cell viability assay, the percentage growth inhibition of basal-HEK293 cells for (A) compound **4a**, (B) compound **4c**, and (C) compound **4f**; Table S1. Inhibitory activity (%) of compounds **4a–n** against human Nicotinamide *N*-methyltransferase (hNNMT) at 10 μM; Table S2. Interactions between hNNMT (6CHH) and **MS2734**, **MvH45** and **4a–n**. Reference [38] is cited in the supplementary materials.

References

1. Trammell, S.A.; Brenner, C. NNMT: A bad actor in fat makes good in liver. *Cell Metab.* **2015**, *22*, 200–201. [CrossRef]
2. Aksoy, S.; Szumlanski, C.L.; Weinshilboum, R.M. Human liver nicotinamide N-methyltransferase. cDNA cloning, expression, and biochemical characterization. *J. Biol. Chem.* **1994**, *269*, 14835–14840. [CrossRef]
3. Riederer, M.; Erwa, W.; Zimmermann, R.; Frank, S.; Zechner, R. Adipose tissue as a source of nicotinamide N-methyltransferase and homocysteine. *Atherosclerosis* **2009**, *204*, 412–417. [CrossRef]
4. Parsons, R.B.; Smith, M.-L.; Williams, A.C.; Waring, R.H.; Ramsden, D.B. Expression of nicotinamide N-methyltransferase (EC 2.1.1.1) in the Parkinsonian brain. *J. Neuropathol. Exp. Neurol.* **2002**, *61*, 111–124. [CrossRef]
5. Williams, A.C.; Ramsden, D.B. Autotoxicity, methylation and a road to the prevention of Parkinson's disease. *J. Clin. Neurosci.* **2005**, *12*, 6–11. [CrossRef]

6. Sartini, D.; Muzzonigro, G.; Milanese, G.; Pierella, F.; Rossi, V.; Emanuelli, M. Identification of nicotinamide N-methyltransferase as a novel tumor marker for renal clear cell carcinoma. *J. Urol.* **2006**, *176*, 2248–2254. [CrossRef]
7. Pissios, P. Nicotinamide N-methyltransferase: More than a vitamin B3 clearance enzyme. *Trends Endocrinol. Metab.* **2017**, *28*, 340–353. [CrossRef]
8. Ramsden, D.B.; Waring, R.H.; Barlow, D.J.; Parsons, R.B. Nicotinamide N-methyltransferase in health and cancer. *J. Tryptophan Res.* **2017**, *10*, 1178646917691739.
9. Lu, X.; Long, H. Nicotinamide N-methyltransferase as a potential marker for cancer. *Neoplasma* **2018**, *65*, 656–663. [CrossRef]
10. Giuliante, R.; Sartini, D.; Bacchetti, T.; Rocchetti, R.; Klöting, I.; Polidori, C.; Ferretti, G.; Emanuelli, M. Potential involvement of nicotinamide N-methyltransferase in the pathogenesis of metabolic syndrome. *Metab. Syndr. Relat. Disord.* **2015**, *13*, 165–170. [CrossRef]
11. Kraus, D.; Yang, Q.; Kong, D.; Banks, A.S.; Zhang, L.; Rodgers, J.T.; Pirinen, E.; Pulinilkunnil, T.C.; Gong, F.; Wang, Y.-c. Nicotinamide N-methyltransferase knockdown protects against diet-induced obesity. *Nature* **2014**, *508*, 258–262. [CrossRef]
12. Milani, Z.H.; Ramsden, D.B.; Parsons, R.B. Neuroprotective Effects of Nicotinamide N-Methyltransferase and its Metabolite 1-Methylnicotinamide. *J. Biochem. Mol. Toxicol.* **2013**, *27*, 451–456. [CrossRef]
13. Ulanovskaya, O.A.; Zuhl, A.M.; Cravatt, B.F. NNMT promotes epigenetic remodeling in cancer by creating a metabolic methylation sink. *Nat. Chem. Biol.* **2013**, *9*, 300–306. [CrossRef]
14. Chen, C.; Wang, X.; Huang, X.; Yong, H.; Shen, J.; Tang, Q.; Zhu, J.; Ni, J.; Feng, Z. Nicotinamide N-methyltransferase: A potential biomarker for worse prognosis in gastric carcinoma. *Am. J. Cancer Res.* **2016**, *6*, 649.
15. Wang, W.; Yang, C.; Wang, T.; Deng, H. Complex roles of nicotinamide N-methyltransferase in cancer progression. *Cell Death Dis.* **2022**, *13*, 267. [CrossRef]
16. Zhang, J.; Wang, Y.; Li, G.; Yu, H.; Xie, X. Down-regulation of nicotinamide N-methyltransferase induces apoptosis in human breast cancer cells via the mitochondria-mediated pathway. *PLoS ONE* **2014**, *9*, e89202. [CrossRef]
17. Neelakantan, H.; Wang, H.-Y.; Vance, V.; Hommel, J.D.; McHardy, S.F.; Watowich, S.J. Structure–Activity Relationship for Small Molecule Inhibitors of Nicotinamide N-Methyltransferase. *J. Med. Chem.* **2017**, *60*, 5015–5028. [CrossRef]
18. van Haren, M.J.; Taig, R.; Kuppens, J.; Toraño, J.S.; Moret, E.E.; Parsons, R.B.; Sartini, D.; Emanuelli, M.; Martin, N.I. Inhibitors of nicotinamide N-methyltransferase designed to mimic the methylation reaction transition state. *Org. Biomol. Chem.* **2017**, *15*, 6656–6667. [CrossRef]
19. Peng, Y.; Sartini, D.; Pozzi, V.; Wilk, D.; Emanuelli, M.; Yee, V.C. Structural basis of substrate recognition in human nicotinamide N-methyltransferase. *Biochemistry* **2011**, *50*, 7800–7808. [CrossRef]
20. Babault, N.; Allali-Hassani, A.; Li, F.; Fan, J.; Yue, A.; Ju, K.; Liu, F.; Vedadi, M.; Liu, J.; Jin, J. Discovery of bisubstrate inhibitors of nicotinamide N-methyltransferase (NNMT). *J. Med. Chem.* **2018**, *61*, 1541–1551. [CrossRef]
21. Kannt, A.; Rajagopal, S.; Kadnur, S.V.; Suresh, J.; Bhamidipati, R.K.; Swaminathan, S.; Hallur, M.S.; Kristam, R.; Elvert, R.; Czech, J. A small molecule inhibitor of Nicotinamide N-methyltransferase for the treatment of metabolic disorders. *Sci. Rep.* **2018**, *8*, 3660. [CrossRef]
22. Gao, Y.; van Haren, M.J.; Buijs, N.; Innocenti, P.; Zhang, Y.; Sartini, D.; Campagna, R.; Emanuelli, M.; Parsons, R.B.; Jespers, W. Potent inhibition of nicotinamide N-methyltransferase by alkene-linked bisubstrate mimics bearing electron deficient aromatics. *J. Med. Chem.* **2021**, *64*, 12938–12963. [CrossRef]
23. Gao, Y.; Martin, N.I.; van Haren, M.J. Nicotinamide N-methyl transferase (NNMT): An emerging therapeutic target. *Drug Discov. Today* **2021**, *26*, 2699–2706. [CrossRef]
24. Yoshida, S.; Uehara, S.; Kondo, N.; Takahashi, Y.; Yamamoto, S.; Kameda, A.; Kawagoe, S.; Inoue, N.; Yamada, M.; Yoshimura, N. Peptide-to-Small Molecule: A Pharmacophore-Guided Small Molecule Lead Generation Strategy from High-Affinity Macrocyclic Peptides. *J. Med. Chem.* **2022**, *65*, 10655–10673. [CrossRef]
25. Payne, M.; Bottomley, A.L.; Och, A.; Hiscocks, H.G.; Asmara, A.P.; Harry, E.J.; Ung, A.T. Synthesis and biological evaluation of tetrahydroisoquinoline-derived antibacterial compounds. *Bioorg. Med. Chem.* **2022**, *57*, 116648. [CrossRef]
26. Alvim-Gaston, M.; Grese, T.; Mahoui, A.; Palkowitz, A.D.; Pineiro-Nunez, M.; Watson, I. Open Innovation Drug Discovery (OIDD): A potential path to novel therapeutic chemical space. *Curr. Top. Med. Chem.* **2014**, *14*, 294–303. [CrossRef]
27. van Haren, M.J.; Sastre Torano, J.; Sartini, D.; Emanuelli, M.; Parsons, R.B.; Martin, N.I. A rapid and efficient assay for the characterization of substrates and inhibitors of nicotinamide N-methyltransferase. *Biochemistry* **2016**, *55*, 5307–5315. [CrossRef]
28. Roberti, A.; Tejedor, J.R.; Díaz-Moreno, I.; López, V.; Santamarina-Ojeda, P.; Pérez, R.F.; Urdinguio, R.G.; Concellón, C.; Martínez-Chantar, M.L.; Fernández-Morera, J.L. Nicotinamide N-methyltransferase (NNMT) regulates the glucocorticoid signaling pathway during the early phase of adipogenesis. *Sci. Rep.* **2023**, *13*, 8293. [CrossRef]
29. Morris, G.M.; Huey, R.; Lindstrom, W.; Sanner, M.F.; Belew, R.K.; Goodsell, D.S.; Olson, A.J. *User Guide, AutoDock Version 4.2, Updated for Version 4.2.6, Automated Docking of Flexible Ligands to Flexible Receptors*; The Scripps Research Institute: San Diego, CA, USA, 2014; Volume 6.
30. Huey, R.; Morris, G.M.; Forli, S. *Using AutoDock 4 and Vina with AutoDockTools: A Tutorial*; The Scripps Research Institute: San Diego, CA, USA, 2011.
31. Forli, S.; Huey, R.; Pique, M.E.; Sanner, M.F.; Goodsell, D.S.; Olson, A.J. Computational protein–ligand docking and virtual drug screening with the AutoDock suite. *Nat. Protoc.* **2016**, *11*, 905–919. [CrossRef]

32. Bock, V.D.; Hiemstra, H.; Van Maarseveen, J.H. CuI-catalyzed alkyne–azide "click" cycloadditions from a mechanistic and synthetic perspective. *Eur. J. Org. Chem.* **2006**, *2006*, 51–68. [CrossRef]
33. Worrell, B.; Malik, J.; Fokin, V. Direct evidence of a dinuclear copper intermediate in Cu (I)-catalyzed azide-alkyne cycloadditions. *Science* **2013**, *340*, 457–460. [CrossRef]
34. Morris, G.M.; Huey, R.; Lindstrom, W.; Sanner, M.F.; Belew, R.K.; Goodsell, D.S.; Olson, A.J. AutoDock4 and AutoDockTools4: Automated docking with selective receptor flexibility. *J. Comput. Chem.* **2009**, *30*, 2785–2791. [CrossRef]
35. Rangsinth, P.; Sillapachaiyaporn, C.; Nilkhet, S.; Tencomnao, T.; Ung, A.T.; Chuchawankul, S. Mushroom-derived bioactive compounds potentially serve as the inhibitors of SARS-CoV-2 main protease: An in silico approach. *J. Tradit. Complement. Med.* **2021**, *11*, 158–172. [CrossRef]
36. Gibbs, J.W. A method of geometrical representation of the thermodynamic properties by means of surfaces. In *The Collected Works of J. Willard Gibbs, Ph. D., LL. D*; Yale University Press: New Haven, CT, USA, 1957; pp. 33–54.
37. Gao, Y.; Van Haren, M.J.; Moret, E.E.; Rood, J.J.; Sartini, D.; Salvucci, A.; Emanuelli, M.; Craveur, P.; Babault, N.; Jin, J. Bisubstrate inhibitors of nicotinamide N-methyltransferase (NNMT) with enhanced activity. *J. Med. Chem.* **2019**, *62*, 6597–6614. [CrossRef]
38. Sauve, A.A. NAD+ and vitamin B3: From metabolism to therapies. *J. Pharmacol. Exp. Ther.* **2008**, *324*, 883–893. [CrossRef]